CI&CEQ
Chemical Industry & Chemical Engineering Quarterly

Available online at
Association of the Chemical Engineers of Serbia AChE
www.ache.org.rs/CICEQ

Chem. Ind. Chem. Eng. Q. 32 (4) xxx–xxx (2026) CI&CEQ

PRADEEP KUMAR GUNASEKARAN[1]
http://orcid.org/0000-0001-9735-1373
THANIGAIVELAN RAJASEKARAN[2]
http://orcid.org/0000-0001-9514-9120
VISWANATHAN RANGASAMY[3]
http://orcid.org/0000-0001-5007-3302

[1]Department of Mechanical Engineering, AVS College of Technology, Salem, India

[2]Department of Mechanical Engineering, Shreenivasa Engineering College, Bommidi, Dharmapuri, India

[3]Department of Mechanical Engineering, AVS Engineering College, Salem, India

SCIENTIFIC PAPER

UDC

ELECTROCHEMICAL MACHINING WITH ETHYLENE GLYCOL MIXED ELECTROLYTE ON INCONEL 718

Highlights

- An ethylene glycol with the combination of $NaNO_3$ has been considered as an electrolyte.
- Stainless steel electrodes are coated with polyvinyl acetate (PVA) and ceramic paste.
- Optimum for stainless steel electrode: 9 V, 70% duty cycle, 28 g L^{-1} electrolyte.
- Optimum for ceramic-coated electrode: 13 V, 80% duty cycle, 28 g L^{-1} electrolyte.

Abstract

Electrochemical machining is a non-traditional machining process, especially for difficult-to-cut materials. An electrolyte was prepared with ethylene glycol (EG) 30 vol% and distilled water 70 vol% as a solution with the combination of $NaNO_3$, and stainless steel electrodes coated with polyvinyl acetate (PVA) and commercially available ceramic paste. Inconel 718 was used as a workpiece material in this study. L_9 orthogonal array (OA) experiments are conducted for both sodium nitrate ($NaNO_3$) and EG+$NaNO_3$ electrolyte. The process parameters are optimized using Preference Ranking Organisation Method of Enrichment Evaluation (PROMETHEE II) and Artificial Neural Network (ANN). According to the multi-criteria decision-making method, the optimal parameter combination of both electrolytes is stainless steel electrode at 9 V, 70% duty cycle, 28 g·L^{-1} electrolyte concentration and ceramic coated electrode at 13 V, 80% duty cycle, 28 g·L^{-1} electrolyte concentration. The results of PROMETHEE II were verified using the developed ANN architecture. ECM performance was significantly improved by adding EG to the sodium nitrate electrolyte. EG significantly improved the material removal efficiency by increasing the average machining rate (MR) by 69.70%. Concurrently, the diametral overcut (DOC) dropped by roughly 27.4%, indicating a significant improvement in dimensional accuracy. Only a slight rise of about 1.6% was seen in the surface corrosion factor (SCF), indicating that the addition of EG has no negative effects on surface integrity.

Keywords: Ethylene glycol, Ceramic coating, Polyvinylacetate, PROMETHEEII, Artificial neural network.

INTRODUCTION

Electrochemical machining (ECM) is a technique for removing metal by electrochemical action. It is typically used in mass production for materials that are extremely hard to machine using conventional methods. ECM is applied to conductive materials, and it can cut small or oddly shaped angles, complex contours, or cavities in hard and rare metals such as titanium aluminide, Inconel, Waspaloy, high nickel, cobalt, and rhenium alloys [1]. Inconel 718 finds use in a variety of applications, such as turbochargers, exhaust valves, aircraft gas turbines, reciprocating engines, rocket engine parts, heat treatment equipment such as furnace covers, fittings, and heat exchangers, as well as the petrochemical and other sectors. In the ECM tool electrode is considered the cathode, the workpiece is the anode, and the electrolyte is filled between these electrodes, and a potential difference is applied across it. During electrolysis, positive ions move towards the cathode and negative ions move towards the anode through the electrolyte, and electrolysis occurs, resulting in the formation of metal hydroxide in the electrolyte and gets precipitated in the electrolyte. Passive oxide layer development remains a serious difficulty in ECM, dramatically lowering efficiency, precision, and material removal rates, especially

Correspondence: T. Rajasekaran, Department of Mechanical Engineering, Shreenivasa Engineering College, Bommidi, Dharmapuri, India-635301.
Email: tvelan10@gmail.com
Paper received: 5 October 2025
Paper revised: 19 November 2025
Paper accepted: 15 December 2025

https://doi.org/10.2298/CICEQ251005033G

in hard-to-machine, corrosion-resistant materials [2]. To overcome the former limitations, researchers have tried with modified electrolytes. Wang *et al.* [3] have used a pulsed power supply to machine Inconel 718 using a sodium nitrate ($NaNO_3$) electrolyte. A pulse current with a shorter pulse length and period enhanced the profile accuracy. The highest deviations of the machined profile were successfully limited within 0.057 mm, and the surface roughness was *Ra*=0.358 μm. Wang *et al.* [4] have machined titanium alloy and Inconel 718 with $NaNO_3$, and compared the performance for dissolution rate and surface quality. It is found that compared to the β phase, the α phase shows a faster electrochemical dissolution rate for TC17, and good surface quality of *Ra* 0.69 μm is attained at the current density of 160 A cm^{-2}. Ren *et al.* [5] have machined the aero engine component, namely boron and phosphorous doped Inconel 718 alloy, using the $NaNO_3$ electrolyte solution. The anodic behaviour of the modified Inconel 718 alloy in the $NaNO_3$ solution was studied by the polarization curve and electrochemical impedance spectroscopy. The analysis shows that an irregular passivation film on the surface of modified Inconel 718, due to the inhomogeneous grain size, reduces the corrosion resistance. Liu *et al.* [6] have studied the polarization performance of titanium in the sodium chloride (NaCl) and ethylene glycol (EG) electrolyte. The study reveals that the NaCl-containing EG electrolyte is the most prominent electrolyte for EMM of micro holes with improved surface integrity and shape accuracy. This type of electrolyte has a smooth surface, small diameter, and tapered, angled micro holes. Guo *et al.* [7] have studied the effect of EG on Zr metallic glasses in ECM. They reported that pulse time has a great impact on stray corrosion, and the use of EG helps to improve the machining localization. Ao *et al.* [8] have machined the shape memory alloys using NaCl-EG blended electrolyte, and the use of this type of electrolyte reduces the surface oxides and improves the surface smoothness. Sivashankar *et al.* [9] have investigated the use of ECM on magnesium AZ31 alloy with a hollow electrode. The result shows that the highest machining speed of 0.439 μm/s and minimum overcut (OC) of 156 μm was achieved during experiments. The machining was improved by 12% when compared to conventional immersed electrolyte machining with a solid tool. Ravi *et al.* [10] have used a recycled scrap alloy matrix-based workpiece in ECM to determine the effect of process variables on machining rate (MR) and surface corrosion factor (SCF). They considered Preference Ranking Organi-sation Method of Enrichment Evaluation (PROMETHEE-2) and found that 7 V, 60% duty cycle, and 30 g/L electrolyte concentration are the best combination. Sivashankar *et al.* [11] have ECMed galvanized iron (GI) sheets using $NaNO_3$ as the electrolyte. Results indicated that voltage notably influenced both machining rate and OC, with optimal machining rate observed at 12 V, 70% duty cycle, and 20 g/l $NaNO_3$ concentration. Cercal *et al.* [12] have added ascorbic acid to the ECM electrolyte, intending to reduce the sludge formation. Using an acidic solution (pH < 5.0), the reducing agent, ascorbic acid, produced a 90% decrease in sludge bulk. The use of gold nanoparticles, hydrogen peroxide, sodium citrate, and sodium chlorate has improved the MR and average surface roughness of the workpiece significantly [13–15]. The combined use of EG+$NaNO_3$ electrolyte with polyvinyl acetate (PVA) and ceramic-coated electrodes for machining Inconel 718 using an L_9 orthogonal array (OA) has not been thoroughly investigated in any previous work, despite the fact that earlier studies have looked at modified electrolytes and coating-assisted ECM. The type of electrodes, electrolyte concentration, voltage, and duty cycle are considered as input parameters. [16–18]. Additionally, this system has not been evaluated through integrated PROMETHEE-II and ANN optimization. Therefore, the current study offers the first thorough experimental and computational evaluation of EG-assisted ECM for Inconel 718, showcasing its potential to greatly increase MR, reduce diametral overcut (DOC), and reduce SCF.

Theory of ECM with blended electrolyte

In the ECM cathode is stainless steel material coated with PVA and ceramic material, and the workpiece is a nickel-based alloy, namely Inconel 718. The electrolyte is prepared using sodium nitrate salt, and 30 vol% % of EG is added to prepare the brine solution. The electrolyte solution undergoes ionic dissolution as shown below when voltage is applied.

$$NaNO_3 \leftrightarrow Na^+ + NO_3^- \quad (1)$$

$$Ni \rightarrow Ni^{2+} + 2e^- \quad (2)$$

$$Ni^{2+} + NO_3^- \rightarrow NiO + NO_2 \uparrow \quad (3)$$

$$Ni + 2NaNO_3 \rightarrow NiO + 2NO_2 \uparrow \quad (4)$$

$$(CH_2OH)_2 \xrightarrow{[O]} 2HCOOH \quad (5)$$

During electrolysis, the nickel ions are liberated from the workpiece. Within the electrolyte, nickel ions would combine with nitrate ions to form nickel oxide and nitrogen dioxide. The formation of formic acid tends to reduce oxide layers formed during electrochemical machining of nickel-based alloys.

Necessary alterations in electrolyte viscosity, dielectric constant, ion mobility, and oxide film behavior are responsible for the enhanced machining rate, decreased DOC, and decreased surface corrosion seen with the EG+$NaNO_3$ combination. At 25 °C, EG has a much higher viscosity than water. Electrolyte flow through the inter-electrode gap is slowed when EG and $NaNO_3$ are combined because of the increased viscosity. A more stable hydrodynamic boundary layer and more homogeneous mass transfer result from decreased turbulence. By reducing the random detachment of gas bubbles, the boundary layer stabilization suppresses stray current pathways and micro-arcing. This improves machining localization and lessens uncontrolled lateral dissolution by concentrating the current density under the active tool area. This immediately helps the EG-blended electrolyte have a smaller DOC. Large diffuse charge layers at the electrode surfaces are likewise less likely to occur when the dielectric constant is reduced. Moreover, during ECM, Inconel 718 produces a stable passive film with oxides of NiO, Cr_2O_3, and Nb/Ti. Rapid oxygen evolution and high water content encourage the development of thick oxide films in pure $NaNO_3$. Passivation prevents the oxidation of nickel to Ni^{2+} and chromium to Cr^{3+} by nitrate ions. This results in uneven corrosion morphology and a lower MR. Formate radicals and weak organic acids are formed during electrolysis when EG+$NaNO_3$ are introduced. These molecules weaken the film by chelating Ni and Cr ions through chemical interactions with passive oxides. When an electric field is introduced, the oxide layer thins and dissolves more easily.

According to the experimental findings, EG functions as a mild de-passivating agent, enhancing the anodic dissolution kinetics and raising the machining rate by over 70%. The EG-blended electrolyte's reduced water content slows down the development of hydrogen gas at the cathode. The effective electrical contact area rises, current density variations fall, and stray sparking is reduced when there are fewer bubbles. This lowers the SCF and increases machining stability. Because of increased ion mobility, quicker oxide production, increased local heating, and increased turbulence and bubble aggregation, the pure $NaNO_3$ solution maintains a more aggressive anodic environment. Pitting-type corrosion and uneven anodic dissolution patterns are likely to occur under these conditions. Smoother hole walls and a smaller corrosion-affected zone are produced by the EG mix electrolyte, which also lessens the electrolyte's aggressiveness, improves dissolving uniformity, and reduces stray current activity.

EXPERIMENTAL

The experimental setup shown in Figure 1 is used for the machining, which consists of an electrode feeding system, electrolyte replenishing system, and pulse power supply unit. The ECM setup machine structure is made up of mild steel, which consists of a base plate, vertical column, and angle plates. The electrode feeding arrangements were powered by a stepper motor. The electrolyte supply system uses a circulation pump and filter, and the machining chamber is made of perspex material. The pulsed power supply has compatibility to vary voltage, current, and duty cycle. The stainless-steel electrode of diameter 464 μm is coated with PVA and ceramic paste to prevent stray current [19,20]. Inconel 718 is used as a workpiece of a thickness of 500 μm. The $NaNO_3$ is used as an electrolyte, which is mixed with 30 vol% of EG. The electrolyte solution is prepared by mixing the salt and EG with 1 L of distilled water. The inter-electrode gap is maintained at 24 μm. The input process variables are the type of electrodes, electrolyte concentration, voltage, and duty cycle, and the output responses are MR, DOC, and SCF. The OA experiment (L_9) is used for conducting the experiments [1]. Two sets of experiments were conducted, one without glycol addition and the other with glycol addition, and experimental details are provided in Tables 1 and 2. Each experiment is repeated twice. Figure 2 shows the three types of tool electrodes used for the experiments. The MR is derived by dividing the thickness of the workpiece by the time taken to complete the hole in the workpiece. The evolution of bubbles beneath the workpiece during the machining process indicates the completion of the hole. The DOC is the difference between the hole diameter at the entry side and the diameter of the tool electrode. The SCF is the ratio of the length of the corrosion on the circumference surface to the diameter of the entry side hole.

THE PROMETHEE II Method

A multi-criteria decision-making (MCDM) method known as PROMETHEE-2 outranks characteristics mostly based on a favorability function strategy. A PROMETHEE-II is intended to generate a comprehensive rating of options. This technique is particularly helpful in engineering, environmental management, logistics, finance, and resource optimization. It may assess options based on several competing criteria (qualitative or quantitative). Preference functions that express how strongly one choice is preferred over another can be used with this method. This flexibility guarantees that the final ranking accurately represents how researchers make decisions in the actual world.

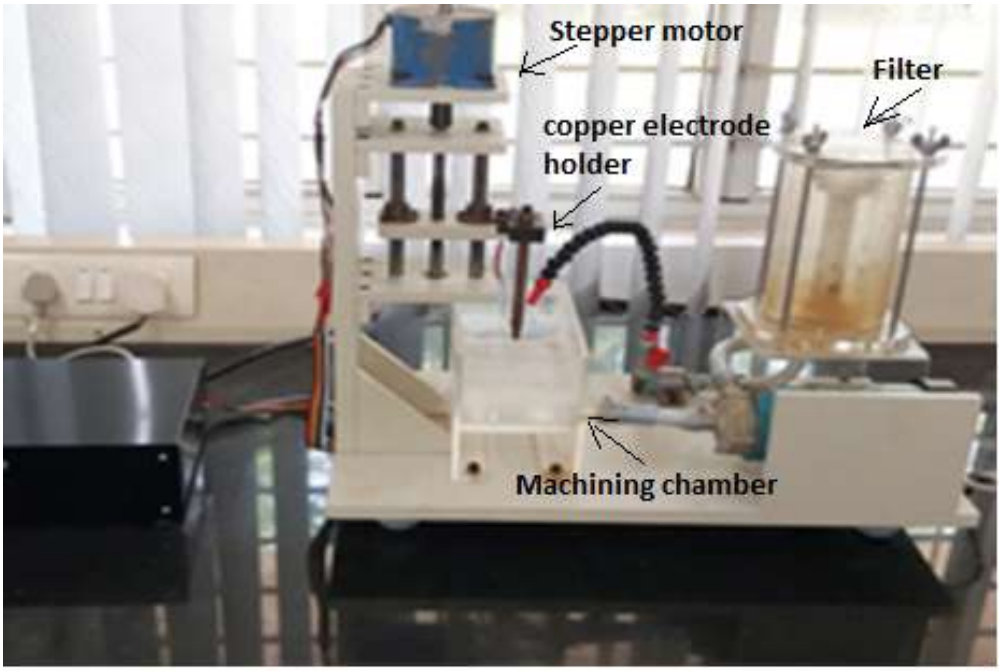

Figure 1. ECM Setup.

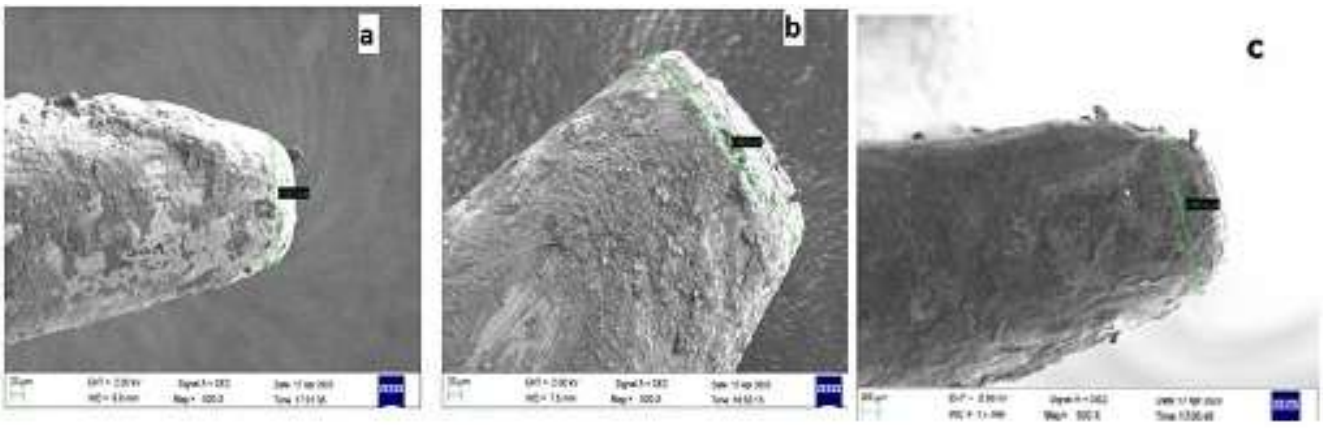

Figure 2. SEM images of tool electrodes.

Table 1. L_9 experiments with sodium nitrate electrolyte without EG.

Expt. No	Type of Tool	CoE (g L^{-1})	V (Volts)	DC (%)	MR (μm s^{-1})	DOC (μm)	SCF	STDEV		
								MR (μm s^{-1})	DOC (μm)	SCF
1	SS	28	9	70	0.238	476	1.21	0.0007	4.51	0.01
2	SS	30	11	80	0.269	516	1.20	0.0007	5.51	0.01
3	SS	32	13	90	0.298	656	1.09	0.0008	6.02	0.01
4	PVA	28	11	90	0.298	426	1.14	0.0012	5.51	0.01
5	PVA	30	13	70	0.253	410	1.21	0.0011	2.52	0.01
6	PVA	32	9	80	0.269	392	1.27	0.0004	8.74	0.01
7	Ceramic	28	13	80	0.309	318	1.28	0.0005	5.51	0.01
8	Ceramic	30	9	90	0.287	326	1.23	0.0052	3.61	0.01
9	Ceramic	32	11	70	0.287	356	1.16	0.0016	8.02	0.01

CoE – Concentration of electrolyte, V – Voltage, DC – Duty Cycle, MR – Machining Rate, DOC – Diametral overcut, and SCF – Surface corrosion factor.

Table 2. L_9 experiments with sodium nitrate electrolyte with EG.

Expt. No	Type of Tool	CoE (g·L^{-1})	V (Volts)	DC (%)	MR (μm.s^{-1})	DOC (μm)	SCF	STDEV		
								MR (μm.s^{-1})	DOC (μm)	SCF
1	SS	28	9	70	0.490	436	1.17	0.001	12.05	0.004
2	SS	30	11	80	0.556	416	1.16	0.001	5.03	0.001
3	SS	32	13	90	0.641	386	1.19	0.008	5.03	0.002
4	PVA	28	11	90	0.397	326	1.16	0.002	10.58	0.26
5	PVA	30	13	70	0.463	286	1.26	0.021	3.05	0.02
6	PVA	32	9	80	0.439	256	1.33	0.003	6.00	0.006
7	Ceramic	28	13	80	0.362	236	1.25	0.004	5.03	0.01
8	Ceramic	30	9	90	0.417	246	1.22	0.009	3.46	0.005
9	Ceramic	32	11	70	0.490	226	1.24	0.006	8.08	0.004

The net preference flow figures obtained using PROMETHEE-II are easy to comprehend. This method does not require sophisticated mathematical expertise, hence it is applied in many fields [21-23]. In fact, the preferred criteria function, equivalent factors, and preference function $P_\alpha(i,j)$ all depend on the pairwise dissimilarity Sα between the evaluations $Ea(i)$ and $Ea(j)$ of the alternatives a and b for the criterion α. In Table 3,

thresholds and weights for factors are shown. As with component dα, the maximum value of indifference indicates the largest variance that the assessor deems to be unimportant when comparing two alternatives according to that criterion. Table 3 also provides an arithmetic study of the favourability function and its relationship to Sα for a variety of criterion functions.

Multi-criterion preference index, $\varepsilon(i,j)$, a weighted average of the preference functions $P_\alpha(i,j)$ for all the criteria, is denoted as [24]:

$$\varepsilon(i,j) = \frac{\sum_{\alpha=1}^{\beta} w_\alpha P_\alpha(i,j)}{\sum_{\alpha=1}^{n} w_\alpha} \quad (6)$$

$$\lambda^+(i) = \frac{\sum_A \varepsilon(i,j)}{S-1} \quad (7)$$

$$\lambda^-(i) = \frac{\sum_A \varepsilon(i,j)}{S-1} \quad (8)$$

$$\lambda(i) = \lambda^+(i) - \lambda^-(i) \quad (9)$$

where w_α is the weight given to the criterion α, (i) is the superiority indicator of a in the alternatives set S, (i) is the net ranking of a in the alternatives set S, and β is the number of criteria. The best/appropriate experiment is the one with the highest $\lambda(i)$ value.

Steps of PROMETHEE-2 methodology

- Step 1: Construction of an evaluation matrix, in which the performance of each alternative with regard to each criterion is reported, must be produced with the basic data.
- Step 2: To determine the performance differences (S_α) between each pair of alternatives with respect to each criterion
- Step 3: Choose the type of criterion function, indifference, and first choice threshold values for every criterion
- Step 4: Calculation of combined indices of preferences for each pair of alternatives.
- Step 5: Evaluations of outranking flows.
- Step 6: Calculation of net outranking flows.
- Step 7: Selection of the best alternative having the highest net outranking value $\lambda(i)$.

RESULTS AND DISCUSSION

The method followed for the calculation of λ and ranking for PROMETHEE-2 is presented in the following steps for both experiments.

Step 1. Table 4 displays the modified payoff matrix along with the number of possibilities, criteria, and payoff matrices that are involved.

Step 2: Pairwise dissimilarity of all values of alternatives for every 9 criteria of Table 4 is estimated. The alternatives X_1 and X_2 give the pairwise dissimilarity value as (0.2381) - (0.2688) = -0.0307. Similarly, pairwise dissimilarity between the alternatives X_2 and X_1 for A_1 is (0.2688) - (0.2381) = 0.0307. Pairwise dissimilarity between the same alternatives X_1 against X_1 is zero. Similarly, for all criteria, A_1 to A_3, are to be calculated. The same procedure is followed for the calculation of criterion A_1 to A_3 for Table 4.

Step 3: Preference function values 1 and 0 are calculated as given below.

For X_1, the usual criterion function is considered for calculating the preference function value. In this, the pairwise dissimilarity between alternatives X_1 and X_2 is (0.2381) - (0.2688) = -0.0307, and the corresponding preference function value is 0. Also, for X_2 to X_1, pairwise dissimilarity is 0.0307, and the corresponding preference function value is selected as 1.

For a formal criterion function, elements of the preference function matrix are 0 or 1. As per Table 4, the pairwise dissimilarity between alternatives X_1-X_2 and X_2-X_1 is -0.0654 and 0.0654, respectively, and hence, the preference function values are 0 and 1.

Pairwise dissimilarity between options X_1 and X_2 for the criterion A_2 is (-476) - (-516) = 40 for the quasi-criterion function for A_2, and the indifference threshold is d = 10. Based on the quasi-criterion function (40 > 10), the preference function value is 1. The preference function value is 0 based on the quasi-criterion function (-40<10) since the differences between options X_2 and X_1 are also (-516) - (-476) = -40. Similar to Table 4, where the preferred values for X_1-X_2 and X_2-X_1 are 0 and 1, respectively.

Step 4: $\varepsilon(i,j)$ is calculated by Eq. (6), and the equivalent weight of each criterion is 0.3333.

Step 5: Estimation of $\lambda^+(i)$, $\lambda^-(i)$ and $\lambda(i)$ as per Eqs. 7-9.

The ranking order of options X_1 to X_2 is 1, 2, and alternative X_1 with the highest value of 0.5833 is selected as the best combination or optimal combination, as is seen from Table 5. According to the analysis, the stainless steel electrode at 9 V, 70% duty cycle, and 28 g·L^{-1} electrolyte concentration is the first optimal factor level, and the second best factor level is stainless steel electrode at 11 V, 80% duty cycle, and 11 g·L^{-1}. The anodic dissolution rate in ECM is regulated by the applied voltage. The potential is strong enough at 9 V to encourage steady electrochemical reactions without producing unintended consequences like sparking, excessive heating, or uncontrollable disintegration. While lower voltages cause slow machining and insufficient material removal, higher voltages frequently result in overcut, poor surface quality, or passivation breakdown.

Therefore, 9 V offers the perfect balance between material removal efficiency, reducing DOC, and SCF. The pulse ON-time is long enough to sustain the workpiece's continuous disintegration at 70% duty cycle. The removal of reaction byproducts is made possible by the 30% OFF-time. While a greater duty cycle may result in inadequate electrolyte cleansing, pitting, and loss of machining precision, a lower duty cycle may lower the material removal rate. Therefore, 70% ensures the best possible balance between machining stability, DOC, and SCF. The electrolyte offers enough ionic strength at 28 g L^{-1} to sustain steady current densities. While lower concentrations result in unstable machining and inadequate dissolution, higher concentrations frequently cause aggressive machining, corrosion, and decreased accuracy. Therefore, the ideal concentration for preserving machining accuracy, consistency, and control is 28 g L^{-1}.

Table 3. Thresholds and weights for factors [14].

Criteria code	Criteria	Criterion function	Thresholds	Normalized weights
A_1	Machining rate	Normal criterion	-	0.3333
A_2	Diametral overcut	Quasi criterion	Indifference d_α = 10	0.3333
A_3	Surface corrosion factor	Normal criterion	-	0.3333

Table 4. Transformed payoff matrix.

Without EG			With EG		
MR (μm·s^{-1})	DOC (μm)	SCF	MR (μm·s^{-1})	DOC (μm)	SCF
0.2381	-476	-1.21	0.490	-436	-1.17
0.2688	-516	-1.20	0.556	-416	-1.16
0.2976	-656	-1.09	0.641	-386	-1.19
0.2976	-426	-1.14	0.397	-326	-1.17
0.2525	-410	-1.21	0.463	-286	-1.26
0.2688	-392	-1.27	0.439	-256	-1.36
0.3086	-318	-1.28	0.362	-236	-1.25
0.2874	-326	-1.23	0.417	-246	-1.22
0.2874	-356	-1.16	0.490	-226	-1.24

Table 5. Ranking pattern for alternatives.

$\lambda^+(i)$	$\lambda^-(i)$	$\lambda(i)$	Rank	$\lambda^+(i)$	$\lambda^-(i)$	$\lambda(i)$	Rank
0.792	0.208	0.58	1	0.50	0.5	0.00	-
0.625	0.333	0.29	2	0.33	0.67	-0.33	-
0.375	0.583	-0.21	-	0.375	0.63	-0.25	-
0.292	0.667	-0.38	-	0.54	0.46	0.08	-
0.625	0.375	0.25	3	0.58	0.33	0.25	2
0.625	0.333	0.29	2	0.58	0.42	0.17	3
0.333	0.625	-0.29	-	0.625	0.30	0.33	1
0.375	0.542	-0.17	-	0.46	0.5	-0.04	-
0.292	0.667	-0.38	-	0.33	0.54	-0.21	-

Based on Table 8, the first best optimal combination is a ceramic-coated electrode at 13 V, 80% duty cycle, and 28 g·L^{-1} electrolyte concentration and the second best combination is the PVA-coated electrode with 13 V, 70% duty cycle, and 30 g·L^{-1} electrolyte concentration. Electrical insulation is introduced by a ceramic-coated electrode, except for micro-exposed tool edges and purposefully exposed conductive zones. This insulation reduces the effective active electrode surface, which lowers the current density at a given voltage and necessitates a higher voltage to induce enough anodic dissolution of the workpiece. Higher electric field strength, uniform breakdown of passive layers on the workpiece, better dissolution under the limited active tool area, and steady machining without arcing are all provided by 13 V. Despite the decreased active area, a prolonged pulse ON-time (80% duty cycle) guarantees that the dissolving reaction proceeds efficiently. Overheating, stray corrosion, and accuracy loss can happen at duty cycles that are too high (>90%). Consequently, the ideal percentage is 80%, which results in robust, long-lasting disintegration. The resistance in the electrochemical gap is raised by the ceramic covering. This is mitigated by a concentration of 28 g L^{-1}, which increases ionic conductivity to sustain a steady current density. Therefore, when utilizing a ceramic-coated tool, 28 g L^{-1} is the ideal concentration to provide a balanced, regulated dissolution process. On comparing the values from Tables 1 and 2, it

is evident that the machining rate, diametral overcut, and surface corrosion factor are on the higher side for the normal electrolyte. The use of EG in $NaNO_3$ reduces the anodic oxide generation on the nickel surfaces that hinders the dissolution process. Moreover, the high viscosity nature of EG settles down the debris generated during machining and also slows down the etch rate. In case of using the $NaNO_3$ electrolyte, the dissolution speed will be higher, and therefore it becomes complex to control the surface features as presented in Figure 3. The figure shows the surface pitting, oxide region, and attachment of debris. In the case of EG, the gas bubble generation at the cathode is reduced, and the instance of stray current and spark generation is reduced. With low water quantity in the electrolyte, the hydrogen generation from the cathode and oxygen generation from the anode are reduced, resulting in a high focused current density, leading to a higher machining rate, lesser overcut, and reduced surface corrosion.

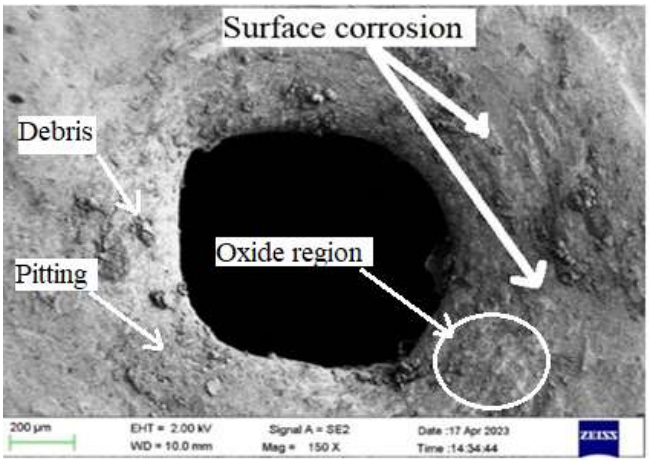

Figure 3. SEM image of the machined hole with pitting, debris, and oxide regions.

ANN OPTIMIZATION

ANN architecture was created with the help of MATLAB'15 to validate the PROMETHEE-2 results. In ANN, a 4 (10) 1 form of architecture gives highly accurate results for the factor optimization [24-29]. The ANN model developed was trained with experimental results and included in MATLAB. To train the ANN model, training values, objective, and test outputs were used. To obtain highly optimum results, 5000 iterations were required. The ANN model consists of two layers, i.e. hidden layer and the output layer.

The ANN architecture consists of four neurons in the input layer (tool type, electrolyte concentration, voltage, duty cycle), ten neurons in the hidden layer, and three neurons in the output layer (MR, DOC, and SCF). The output layer is purelin (linear), and the hidden layer's activation function is tansig (hyperbolic tangent sigmoid). The training algorithm uses the mean squared error as the loss function and Levenberg-Marquardt backpropagation (trainlm), with an epoch limit of 5000 and a performance objective of 1×10^{-2}. Because of its quick convergence on small and medium-sized datasets, which are common in L_9 OA-based ECM research, the Levenberg-Marquardt algorithm was chosen. To stabilize training, normalization and cross-condition pairing were added to the dataset (9 experimental points × 2 electrolyte conditions). Using MATLAB, the data was divided at random into 70% training, 15% validation, and 15% testing. Moreover, $R = 0.953$ (training), $R = 0.939$ (validation), $R = 0.949$ (testing), and $R = 0.952$ (overall) were all attained by the trained ANN. The high correlation coefficient confirms excellent predictive alignment between experimental and network-predicted responses. Figure 4 displays an example regression plot that corresponds to the ANN prediction accuracy ($R = 0.95$).

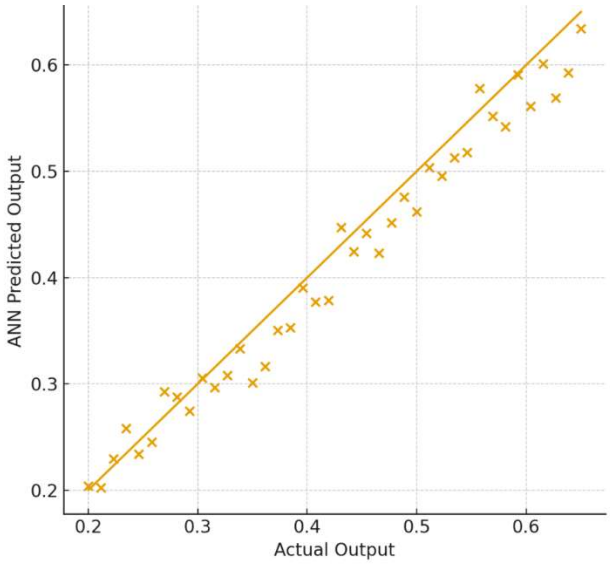

Figure 4. Regression plot for ANN prediction accuracy (R = 0.95).

As per the training, the regression curve was drawn, and the developed model shows an *R*-value of 95.3% for the duration of training. In the developed model, the overall *R*-value was 94.9%. Validation was performed with an *R*-value of 93.9%. On the whole, the developed ANN model shows highly accurate test results. Hence, PROMETHEE-2 prediction results and optimization values were utilised as test values in the trained ANN model. It precisely predicts that the machining rate value is 0.289 µm/s, whereas PROMETHEE-2 optimized the value of 0.238 µm/s for the $NaNO_3$ electrolyte. For the EG-mixed electrolyte, the ANN prediction is 0.374 µm/sand, and the PROMETHEE-2 optimized value is 0.417 µm/s. Moreover, for a normal electrolyte, the DOC predicted through ANN is 652 µm, and the optimized value is 476 µm. The predicted value for the EG mixed electrolyte is 226 µm, and itmatches the optimized value of 236 µm. The prediction for the surface corrosion factor through ANN for both the electrolytes is 1.239 and 1.127, respectively, which is close to the optimized values of 1.213 and 1.246.

As per Table 6, under both electrolytes, ANN predicts SCF with the maximum accuracy (≤10% inaccuracy). A good fit for dynamic dissolving behavior is indicated by machining rate, which displays acceptable prediction errors (10-21%). DOC is heavily impacted by geometric factors and small stray current fluctuations that the small L_9 dataset is unable to fully capture. DOC exhibits the highest variances, particularly for $NaNO_3$ alone. Overall, the ANN model's applicability for ECM parameter prediction is supported by its consistent validation of PROMETHEE-II ranks.

Table 6. Comparison of PROMETHEE-II and ANN Predictions with % Error.

Response	*$NaNO_3$ Electrolyte (without EG)*			EG + $NaNO_3$ Electrolyte		
	PROMETHEE-II (Optimized)	*ANN Prediction*	% Error	*PROMETHEE-II (Optimized)*	*ANN Prediction*	% Error
MR (μm·s^{-1})	0.238	0.289	21.4%	0.417	0.374	10.2%
DOC (μm)	476	652	37.0%	236	226	4.2%
SCF	1.213	1.239	2.1%	1.246	1.127	9.6%

CONCLUSIONS

Experiments using the EG electrolyte and coated electrodes optimized ECM parameters via PROMETHEE-II and ANN. EG improved machining speed, diametral over-cut (DOC), and reduced corrosion compared to $NaNO_3$. PROMETHEE-II ranked stainless steel best at 9 V, 70% duty, and 28 g·L^{-1}, followed by 11 V, 80%, and 11 g·L^{-1}. With EG, the optimum for the ceramic-coated electrode was 13 V, 80%, and 28 g·L^{-1}, followed by the optimum for the PVA-coated electrode, which was 13 V, 70%, and 30 g·L^{-1}. ANN predictions closely matched these results. Predicted machining rates were 0.289 μm s^{-1} ($NaNO_3$) and 0.374 μm s^{-1} (EG) versus the optimized ones of 0.238 and 0.417 μm·s^{-1}. Predicted DOCs (652 μm, 226 μm) were close to optimized (476 μm, 236 μm). Corrosion factors predicted (1.239, 1.127) aligned with optimized (1.213, 1.246). Thus, the EG electrolyte with coated tools enhances ECM performance and prediction accuracy. The practical value of this approach for high-precision machining of nickel-based superalloys like Inconel 718, which are widely used in aerospace turbine components, automotive turbocharg-ers, and energy systems, is highlighted by the demonstra-ted improvements achieved using the EG+$NaNO_3$-blended electrolyte, namely a ~70% increase in machining rate, ~27% reduction in overcut, and lower corrosion. The suggested electrolyte and tool-coating strategy provides an economical and industrially scalable way to reduce tool wear, minimize post-processing, and improve overall production efficiency in advanced manufacturing sectors by facilitating faster, cleaner, and more dimensionally accurate machining.

REFERENCES

[1] R. Thanigaivelan, R.M. Arunachalam, J. Jerald, T. Niranjan, Int. J. Exp. Des. Process Optim. 2 (2011) 283-298. https://doi.org/10.1504/IJEDPO.2011.043565.

[2] R.K. Upadhyay, J. Electrochem. Sci. Eng. 15 (2025) 2796. https://doi.org/10.5599/jese.2796

[3] J. Wang, Z. Xu, T. Geng, D. Zhu, Sci. China Technol. Sci. 65 (2022) 2485-2502. https://doi.org/10.1007/s11431-021-2043-9.

[4] Y. Wang, Z. Xu, D. Meng, Z. Wang, J. Electrochem. Soc. 168 (2021) 073502. https://doi.org/10.1149/1945-7111/ac131a.

[5] M. Ren, D. Zhu, Z. Li, G. Lei, J. Alloys Compd. 944 (2023) 169140. https://doi.org/10.1016/j.jallcom.2023.169140.

[6] W. Liu, H. Zhang, Z. Luo, C. Zhao, S. Ao, F. Gao, Y. Sun, J. Mater. Process. Technol. 255 (2018) 784-794. https://doi.org/10.1016/j.jmatprotec.2018.01.009.

[7] C. Guo, B. Wu, B. Xu, S. Wu, J. Shen, X. Wu, Electrochem. Soc. 168 (2021) 071502. https://doi.org/10.1149/1945-7111/ac0bf8.

[8] S. Ao, K. Li, W. Liu, X. Qin, T. Wang, Y. Dai, Z. Luo, J. Manuf. Process. 53 (2020) 223-228. https://doi.org/10.2298/CICEQ211204007V.

[9] N. Sivashankar, R. Thanigaivelan, L. Selvarajan, K. Venkataramanan, Ultrasonics, 147 (2025) 107526. https://doi.org/10.1016/j.ultras.2024.107526

[10] V.P. Ravi, R.A. Sankaran, Bull. Chem. Soc. Ethiop. 38 (2024) 1163-1175. https://doi.org/10.4314/bcse.v38i4.27

[11] N. Sivashankar, K. Santhanam, S. Prasad, M. Jawahar, R. Thanigaivelan, J. Electrochem. Sci. Eng. (2025) 2821. https://doi.org/10.5599/jese.2821

[12] G. Cercal, G. de Alvarenga, M. Vidotti, Processes,11 (2023), 2186. https://doi.org/10.3390/pr11072186

[13] R.K. Upadhyay, A.K. Chakraborty, S.S. Majhi, Ashish C. Singh, Bishnu Kumar, Narendra Yadav. Surf. Sci. Technol. 3 (2025) 11. https://doi.org/10.1007/s44251-025-00074-9

[14] S. Ayyappan, K. Sivakumar, Int J Adv Manuf Technol 82 (2016) 2053-2064 https://doi.org/10.1007/s00170-015-7511-6

[15] L. Guodong, L. Yong, K. Quancun, K., T. Hao, Procedia CIRP, 42 (2016) 412-417. https://doi.org/10.1016/j.procir.2016.02.223

[16] R. Manivannan, T. Niranjan, S. Maniraj, R. Thanigaivelan, J. New Mater. Electrochem. Syst. 27 (2024) 25-29. https://doi.org/10.14447/jnmes.v27i1.a04.

[17] K. Gunasekaran, G. Pradeep Kumar, R. Thanigaivelan, R. Arunachalam, V. Shanmugam, J. New Mater. Electrochem. Syst. 24 (2021) 49-54. https://doi.org/10.14447/jnmes.v24i1.a09.

[18] B. Babu, C. Sabarinathan, S. Dharmalingam, J. New Mater. Electrochem. Syst. 23 (2020) 94-100. https://doi.org/10.14447/jnmes.v23i2.a06.

[19] R. Thanigaivelan, R.M. Arunachalam, Trans. NAMRI/SME 38 (2010) 253-260. https://www.proceedings.com/content/009/009267webtoc.pdf

[20] M. Soundarrajan, R. Thanigaivelan, Russ. J. Electrochem. 57 (2021) 172-182. https://doi.org/10.1134/S1023193521020117.

[21] P. Annamalai, C. Dhavamani, Trans. Indian Inst. Met. 76 (2023) 1831-1839. https://doi.org/10.1007/s12666-023-02880-x.

[22] S. Javaid, H.T. Gorji, K.B. Soulami, N. Kaabouch, Res. Biomed. Eng. 39 (2023) 129-138. https://doi.org/10.1007/s42600-022-00257-5.
[23] Z. Chergui, Math. Stat. Eng. Appl. 72 (2023) 1544-1559. https://doi.org/10.17762/msea.v72i1.2382.
[24] D. Deepa, R. Thanigaivelan, K. Gunasekaran, S. Praveenkumar, Tec. Ital. 65 (2021) 446-449. https://doi.org/10.18280/ti-ijes.652-444.
[25] N. Sivashankar, R. Thanigaivelan, K.G. Saravanan, Bull. Chem. Soc. Ethiop. 37 (2023) 1263-1273. https://doi.org/10.4314/bcse.v37i5.17.
[26] A. Kosarac, C. Mladjenovic, M. Zeljkovic, S. Tabakovic, M. Knezev, Materials 15 (2022) 700. https://doi.org/10.3390/ma15030700.
[27] D.M.D'Addona, D. Matarazzo, R. Teti, P.R. Aguiar, E.C. Bianchi, A. Fornaro, Procedia CIRP 7 (2013) 323-328. https://doi.org/10.1016/j.procir.2017.03.043.
[28] K.S. Sangwan, S. Saxena, G. Kant, Procedia CIRP 29 (2015) 305-310. https://doi.org/10.1016/j.procir.2015.02.002.
[29] P.K. Nalajam, R. Varadarajan, Exp. Techn. 45 (2021) 705-720. https://doi.org/10.1007/s40799-021-00451-7.
Click or tap here to enter text.

PRADEEP KUMAR GUNASEKARAN[1]

THANIGAIVELAN RAJASEKARAN[2]

VISWANATHAN RANGASAMY[1]

[1]Department of Mechanical Engineering, AVS College of Technology, Salem, India

[2]Department of Mechanical Engineering, Shreenivasa Engineering College, Bommidi, Dharmapuri, India

[3]Department of Mechanical Engineering, AVS Engineering College, Salem, India

NAUČNI RAD

ELEKTROHEMIJSKA OBRADA INCONEL 718 MEŠAVINOM ELEKTROLITA I ETILEN GLIKOLA

Elektrohemijska obrada je netradicionalni proces obrade, posebno za materijale koji se teško seku. Elektrolit je pripremljen kao mešavina 30 vol.% vodenog rastvora etilen-glikola (EG) i $NaNO_3$. Elektroda od nerđajućeg čelika je obložena polivinil-acetatom (PVA) i komercijalno dostupnom keramičkom pastom. Inkonel 718 je korišćen kao materijal za radni predmet. Sprovedeni su eksperimenti sa L_9 ortogonalnim nizom (OA) za $NaNO_3$ i EG+$NaNO_3$. Parametri procesa su optimizovani korišćenjem metode PROMETHEE II i veštačke neuronske mreže (ANN). Prema metodi višekriterijumskog odlučivanja, optimalna kombinacija parametara oba elektrolita je elektroda od nerđajućeg čelika na 9 V, 70% radnog ciklusa i koncentraciji elektrolita od 28 g L^{-1} i elektroda sa keramičkim premazom na 13 V, 80% radnog ciklusa i koncentraciji elektrolita od 28 g L^{-1}. Rezultati PROMETHEE II su verifikovani korišćenjem razvijene arhitekture ANN). Performanse elektrolitskog premaza (ECM) su značajno poboljšane dodavanjem EG u $NaNO_3$. EG je značajno poboljšao efikasnost uklanjanja materijala povećanjem prosečne brzine obrade (MR) za 69,70%. Istovremeno, dijametralno prerezivanje (DOC) je smanjeno za otprilike 27,4%, što ukazuje na značajno poboljšanje dimenzionalne tačnosti. Primećen je samo blagi porast od oko 1,6% u faktoru površinske korozije (SCF), što ukazuje da dodavanje EG nema negativnih efekata na integritet površine.

Ključne reči: Etilen-glikol, keramički premaz, polivinil acetat, PROMETHEEII, veštačka neuronska mreža.